Analysis of thermal stresses in square ducts of solar receivers operated with liquid sodium

F. Gonzalez[1], R. Barraza[1], T. Schaub[2], D. Estay[1], L. Guzman[1]

[1] Departamento de ingeniería mecánica/Universidad Técnica Federico Santa María, Chile

[2] Karlsruhe Institute of Technology/Germany

Abstract

One of the failures in the solar receivers is usually produced by thermal stresses caused by the non-uniformity of the concentrated solar flux and the transient behavior of the climate. The use of liquid sodium as a heat transfer fluid allows to reach higher temperatures to feed more efficient power systems, however, this produces an increase in thermal stresses, putting the safety of the facilities at risk. The change of geometry is an alternative to improve the thermo-mechanical behavior of the receiver tubes. To compare the thermal and hydraulic characteristics, parameters such as the Reynolds number, the pressure loss, the internal heat transfer coefficient, and the mass flow are determined. With these, six equivalences are tested between conventional tubes and square ducts. The results show that for all the conditions of equivalence the thermal stress increases in comparison with a conventional tube, specifically in the corners of the square duct, however, the characteristics of heat transfer and pressure drop can be maintained and improved. These results imply that the use of other geometries can benefit the overall efficiency of the receiver as well as affect the levelized cost of electricity (LCOE).

Keywords: Concentrated solar power, liquid sodium, thermal stress, receiver

1. Introduction

In the field of solar energy, concentrated solar plants (CSP) are of great interest in terms of generated energy compared to photovoltaic or wind plants because of the higher plant factors they reach. Also, research on new power blocks, such as supercritical CO_2, requires working fluid to reach temperatures above $700\ °C$ (Besarati and Goswami, 2017). Using a liquid metal such as sodium provides wider operating temperature ranges compared to other fluids such as molten salts or steam (Ho, 2017), this makes it possible to use more efficient power cycles and generate more energy.

One of the most common failures of the receiver tubes is produced by thermal stresses that exceed the elastic limit of the material. The thermal stress may have cyclical behavior due to the passage of clouds or the weather conditions of the place; these transient changes may cause temperature rise to the average melting temperature inducing the flow of the material. The permanent presence of creep and fatigue produces plastic deformations to the metal, which in the long term, causes the failure and the decrease of the lifespan of the receiver (Rodriguez-Sanchez et al., 2014)

In this context, there are authors who relate the thermal stresses in sodium-operated solar receivers (Conroy et al., 2018a; Conroy et al., 2018b; Logie et al., 2018; Cagnioli et al., 2019; Boerema et al., 2013), in these research, it can be concluded how the thermal stress decreases compared to a receiver operated with molten salts, given the high thermal conductivity and heat transfer rate of liquid sodium. Of these authors, only Boerema includes the change of dimensions and arrangement of the tubes. However, the use other types of geometries such as square ducts, has not been fully explored. The interest to use other ducts geometries begins from the presence of secondary flows in ducts with sharp corners that modify the average behavior of the fluid velocity and tend to increase the heat transfer from the corners to the fluid (Kakac et al 1987). According to the review of the state of the art and the previously presented authors, studies showing the effect of changing the profiles of the

doi:10.18086/swc.2019.01.04 Available at http://proceedings.ises.org

solar receiver tubes are scarce. In this document, the comparison of the cross-section of circular tubes with square ducts of a sodium-operated solar receiver is made through a 2D model programmed in Matlab. The contribution of this research allows laying the foundations for the design of a receiver that has a thermo-elastic performance similar or better than conventional receivers.

2. Methodology

The solar receiver billboards are formed by circular tubes in parallel, therefore, the approach to model the tube is to consider it as a series of segments of finite cross-sections where the temperature of each segment can change in the x- and y-axis but does not change on the z-axis perpendicular to the cross section.

It should be noted that for this analysis, the interaction between the adjacent tubes, is not considered. The scheme of the problem is shown in Fig. 1. In this one, the average temperature of the fluid T_{htf} is constant inside the tube and the flow of incident radiation on the front of the tube q_{inc}. is also uniform. For purposes of comparison with other geometries, the problem is solved in cartesian coordinates.

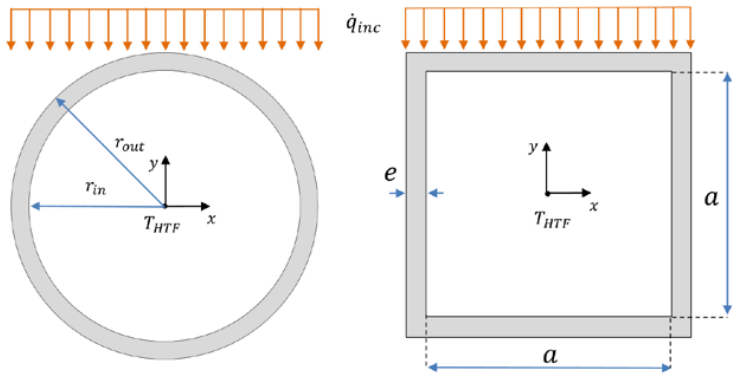

Fig. 1: Cross-section of the tubes with the flow of radiation from the front, fluid circulating inside and with adiabatic condition from the back

2.1 Temperature Distribution

It assumes that the temperature distribution in the cross-section of the tube is in a steady-state and can be obtained with the Laplace equation

$$\frac{\partial^2 T}{\partial x^2} + \frac{\partial^2 T}{\partial y^2} = 0 \qquad \text{(eq. 1)}$$

The boundary conditions for the exterior front part, are expressed as a function of a unit vector normal to the surface $\vec{n}_o$

$$k_t \left.\frac{\partial T}{\partial n}\right|_{\vec{n}_o} = \alpha \vec{q}_{inc} \cdot \vec{n}_o + \epsilon\beta(T_o^4 - T_\infty^4) + h_o(T_o - T_\infty) \qquad \text{(eq. 2)}$$

Where k_t is the thermal conductivity, α is the absorptivity of the surface, ϵ the emissivity, β is the Stephan-Boltzmann constant, $\vec{q}_{inc}$ the solar concentrated flux and h_o is the external heat transfer coefficient. The outside temperature is T_o and the ambient temperature is T_∞

Inside the tube, the boundary condition for temperature corresponds to forced internal convection and acts in $\vec{n}_i$ direction

$$k_t \frac{\partial T}{\partial n}\Big|_{\vec{n}_i} = h_i(T_i - T_{htf}) \quad \text{(eq. 3)}$$

The internal heat transfer coefficient h_i is obtained with the thermal conductivity of the fluid (k), the characteristic length (L) and Nusselt number (Nu)

$$h_i = Nu \cdot \frac{k}{L} \quad \text{(eq. 4)}$$

2.2 Thermal Stress

To obtain the stress distribution in the cross-section of the tube, the flat deformation condition ($\varepsilon_z = 0$) will be used. Hooke's law establishes the relationship between deformations and stress.

$$\sigma = [R](\varepsilon - \varepsilon_0) \quad \text{(eq. 5)}$$

Where the matrix $[R]$ contains the elastic properties such as the Young modulus (E) and the Poisson modulus (ν).

$$[R] = \frac{E}{(1-\nu)(1-2\nu)}\begin{pmatrix} 1-\nu & \nu & 0 \\ \nu & 1-\nu & 0 \\ 0 & 0 & (1-2\nu)/2 \end{pmatrix} \quad \text{(eq. 6)}$$

The term ε_0 correspond to the initial deformations, which in this case, are the thermal deformations ε_T.

$$\varepsilon_T = \begin{pmatrix} (1+\nu)\lambda\Delta T \\ (1+\nu)\lambda\Delta T \\ 0 \end{pmatrix} \quad \text{(eq. 7)}$$

Where λ is the coefficient of linear expansion and ΔT is the temperature difference ($T - T_0$), with T_0 the stress-free temperature that for metals is considered at ambient temperature ($20\,°C$). Therefore, the relationship between stress and deformation for this problem is as follows:

$$\begin{pmatrix} \sigma_x \\ \sigma_y \\ \sigma_{xy} \end{pmatrix} = [R]\begin{pmatrix} \varepsilon_x - (1+\nu)\lambda\Delta T \\ \varepsilon_y - (1+\nu)\lambda\Delta T \\ \gamma_{xy} \end{pmatrix} \quad \text{(eq. 8)}$$

3. Verification

For the purposes of code verification, the results presented by Logie (Logie et al., 2018) will be used, the parameters used are listed in Tab 1.

Tab 1: Parameters used for verification (Logie et al., 2018)

Property	Unit	Value
T_{htf}	$°C$	450
Nu		19.6
h_i	$kW^{-2}K^{-1}$	43.6
r_i	mm	15.05
r_o	mm	16.7
q_{inc}	kWm^{-1}	850
E	MPa	165
ν		0.3
k	$Wm^{-1}K^{-1}$	20
λ	K^{-1}	$18.5 \cdot 10^{-6}$

For comparison and analysis purposes, the Von Mises equivalent stress is calculated, according to the failure theory, this equivalent stress must be less than the yield stress to ensure that the material remains in the zone of elasticity and plastic deformation failures do not occur.

In the case of stainless steels suitable for the use of liquid sodium SS304L and SS316 L, the yield stress is 170 MPa.

$$\sigma_{vm} = \sqrt{\frac{(\sigma_x - \sigma_y)^2 + (\sigma_y - \sigma_z)^2 + (\sigma_z - \sigma_x)^2}{2} + 6\tau_{xy}} \quad \text{(eq. 9)}$$

The semi-analytical method used by Logie is only proposed for the half of the tube, since the temperature distribution is symmetric with respect to an axis that cuts the cross-section in two, however, the finite element method allows calculating the stress for the entire cross-section. The conditions of zero axial force (Fig. 2) and annulled bending moment (Fig. 3) for both methods are presented.

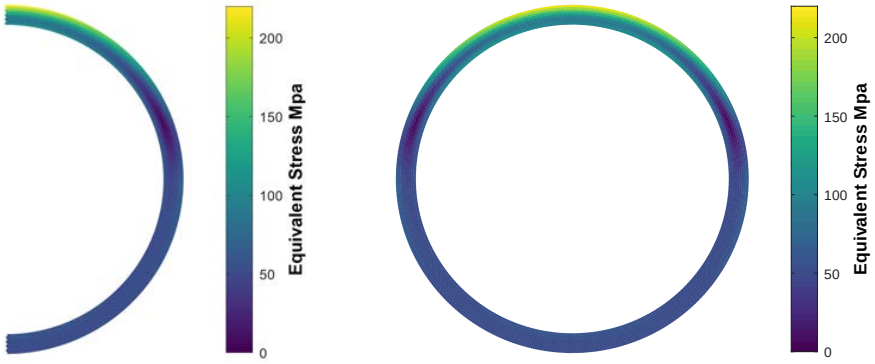

Fig. 2: Equivalent stress for the zero axial force condition (z.a.f) of the cross-section of the tube. Results obtained with the method of Logie et al. (left) and the ones on this study (right).

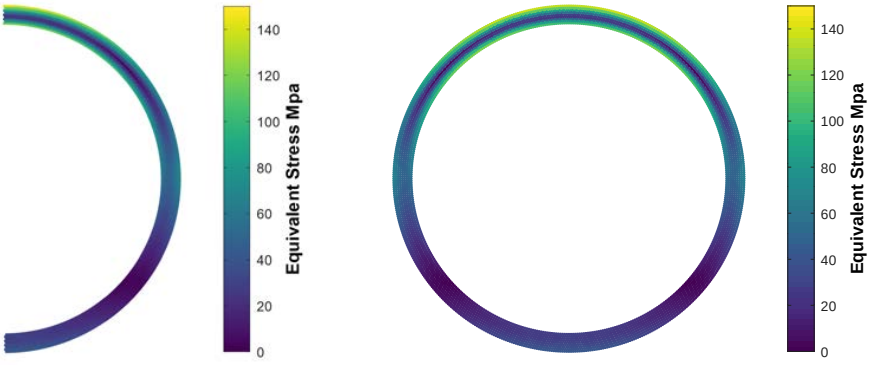

Fig. 3: Equivalent stress for the annulled bending moment condition (a.b.m) of the cross-section of the tube. Results obtained with the method of Logie et al. (left) and the ones on this study (right).

The difference between the semi-analytic method and the finite element method is quantified with the percentage error of the equivalent effort between the common nodes of both cases. The discrepancy shown in Tab.2 may be because the semi-analytic method takes a curve fit for the inside and outside of the tube and then calculates the stresses. With this adjustment, it is assumed that along the radial direction of the tube, there is a distribution similar to the weighting between the inside and outside temperature. On the other hand, the finite element method takes the temperature of each of the nodes and calculates the thermal stress based on the temperature difference with the adjacent nodes.

Tab. 2: Comparison of the maximum equivalent stress for the case of zero axial force (z.a.f) and annulled bending moment (a.b.m)

Method	Semi analytic	*Finite Elements*	Difference %
σ_{max} **Mpa (F.A.N)**	**218**	**212**	**7**
σ_{max} **Mpa (M.F.A)**	**141**	**136**	**12**

4. Geometry Equivalence

The equivalence of geometries corresponds to equating variables that allow comparing different geometries. Dimensionless numbers are useful for this purpose, for example, to maintain the thermal and physical properties of liquid sodium, it is necessary to use the same Prandtl number between two different geometries.

For this problem the variables of interest are the pressure drop ΔP, the mass flow $\dot{m}$, the heat transfer coefficient h, and the Reynolds number (Re). If only one of the variables remains, two unknowns correspond to the fluid velocity and the hydraulic diameter, therefore, it is necessary to set two conditions that allow solving the problem. From the mentioned variables, six equivalence conditions arise that allow finding the diameter of the square ducts and thus proceed to the calculation of the temperature and stress distribution.

5. Results and discussion

For the equivalences the example of the sodium-operated receiver in Vast Solar will be taken, this corresponds to a billboard of 60 tubes of 23 mm in diameter made of 304 stainless steel, with a thickness of 1 mm. Conroy et al. (Conroy et al 2018b) shows the thermo-mechanical effect in the panel of different approach strategies for the heliostat field, the results for a radiation flow of 1.2 MWm^{-2} are shown in Tab. 3

Tab. 3: Results obtained with the parameters of the Vast Solar receiver (Conroy et al. 2018b)

Re	ΔP	$\dot{m}$	h	T_{htf}	σ_{max}
16874	24.5 $Pa\ m^{-1}$	0.077 $kg\ s^{-1}$	15978 $Wm^{-2}K^{-1}$	454 $°C$	139 MPa

Then with the six conditions of equivalence defined in the previous section, the hydraulic diameters for a square tube and the parameters related to its thermo-hydraulic behavior, are obtained.

Tab. 4: Equivalent diameter for square ducts fot the six equivalences of geometries

Equivalence	$D\ mm$	Re	$\Delta P\ Pa/m$	$\dot{m}\ kg/s$	$h\ W/m^2K$	$\sigma_{max}\ MPa$
$\Delta P \setminus Re$	23	16874	24.5	0.098	24019	174
$\Delta P \setminus h$	36	36782	24.5	0.336	15979	176
$\Delta P \setminus \dot{m}$	21	14437	24.5	0.077	26072	174
$Re \setminus h$	35	16874	7.2	0.147	15979	197
$Re \setminus \dot{m}$	18	16874	50.6	0.077	30567	170
$h \setminus \dot{m}$	34	9021	2.5	0.077	15979	212

The hydraulic diameter for a square duct corresponds to the length of one of its sides, therefore, for the same hydraulic diameter of a circular tube and a square duct, the latter, has more area. This implies that the speed of the fluid is different and, consequently, the properties such as the mass flow, the pressure drop, and the heat transfer coefficient change for each combination of equivalence. In engineering terms, maintaining the pressure drop is preponderant, since this implies maintaining the pumping power, therefore, the Reynolds number and the mass flow directly influence this issue, the tube dimensions and thickness impact on the cost of the receiver manufacturing, and the heat transfer coefficient affects the temperature reached by the fluid, consequently, all these parameters determine the Levelized cost of electricity (LCOE).

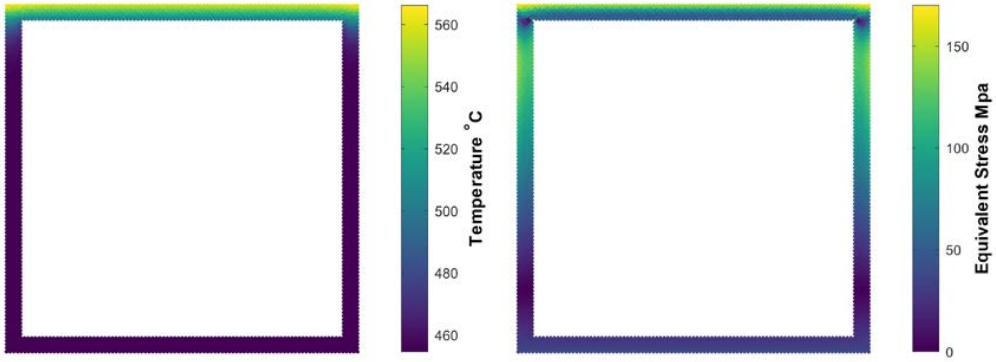

Fig. 4: Temperature distribution (left) and equivalent stress (right) for the annulled bending moment condition of the cross-section of the square duct, for the first equivalence

The risk in using liquid sodium focuses on that the correct choice of geometry is through the effort the tube reaches. For all cases of equivalence shown in Tab. 4, the stress is greater compared with the tubes, specifically in the corners, what it explains, since the internal convection works perpendicular to the inner surface, so that in the corners the flow is not withdrawn in the same way as in the frontal part where the solar radiation flow and the internal convection are in the same direction. According to Fig. 4, the sharp corners obstruct the transfer of heat, which implies that the temperature increases and, consequently, the effort increases. One option is curving the corners both inside and outside and observe how the front exterior temperature profile of the square duct changes.

This effect is shown in Fig. 5; in which it is noted how the temperature peak can decrease when the radii of curvature change. In particular, the greatest decrease is for $r_o = 2\ mm$ - $r_i = 0\ mm$, however this case presents manufacturing problems, therefore, the best combination would be $r_o = 1\ mm - r_i = 0$ mm.

Nevertheless, the decrease in temperature between the case of completely-straight corners and the outline of the outside is small.

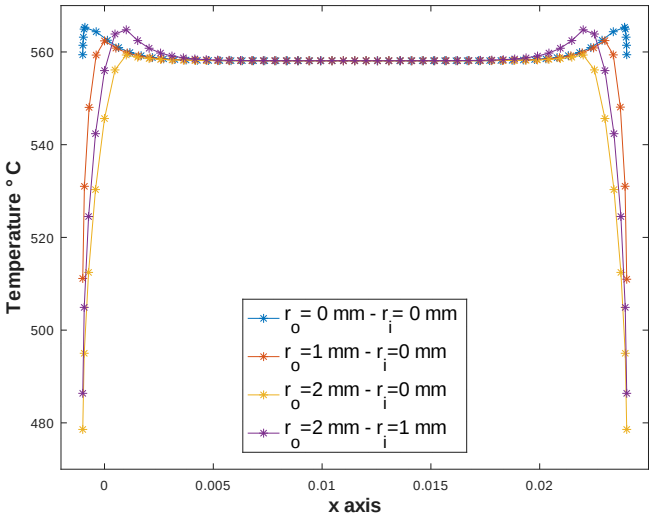

Fig. 5: Effect of the contour of the corners on the outer front profile of temperature for a square duct with the first condition of equivalence

Based on the results found, it is important to consider the effects of the secondary flows, since the coefficient of heat transfer at the corners can contribute to the decrease in temperature peaks. Also, using geometries as square ducts has certain advantages such as the increase of the average heat transfer coefficient that allows to increase the temperature of sodium and thus power more efficient power cycles.

6. Acknowledgement

The author gratefully acknowledges the financial support provided by the Solar energy research center, SERC Chile (CONICYT/15110019) and the DGIIP (“Dirección General de Investigación, Innovación y Postgrado”) supported by “Universidad Tecnica Federico Santa Maria”

7. References

Besarati, S., Goswami, D., 2017. 8 - supercritical co2 and other advanced power cycles for concentrating solar thermal (cst) systems, in: Blanco, M.J., Santigosa, L.R. (Eds.), Advances in Concentrating Solar Thermal Research and Technology. Woodhead Publishing. Woodhead Publishing Series in Energy, pp. 157 - 178.

Boerema, N., Morrison, G., Taylor, R., Rosengarten, G., 2013. High temperature solar thermal central-receiver billboard design. Solar Energy 97, 356 - 368.

Cagnoli, M., de la Calle, A., Pye, J., Savoldi, L., Zanino, R., 2019. A cfd supported dynamic system-level model of a sodium-cooled billboard-type receiver for central tower csp applications. Solar Energy 177, 576 - 594.

Conroy, T., Collins, M.N., Fisher, J., Grimes, R., 2018a. Levelized cost of electricity evaluation of liquid sodium receiver designs through a thermal performance, mechanical reliability, and pressure drop analysis. Solar Energy 166, 472 - 485.

Conroy, T., Collins, M.N., Fisher, J., Grimes, R., 2018b. Thermal and mechanical analysis of a sodium-cooled solar receiver operating under a novel heliostat aiming point strategy. Applied Energy 230, 590 - 614. Fidler,

Ho, C.K., 2017. Advances in central receivers for concentrating solar applications. Solar Energy 152, 38 - 56. Progress in Solar Energy Special Issue: Concentrating Solar Power (CSP).

Kakac, S., Shah, R.K., & Aung, W. (1987). Handbook of single-phase convective heat transfer. Chapter 4.

Logie, W.R., Pye, J.D., Coventry, J., 2018. Thermoelastic stress in concentrating solar receiver tubes: A retrospect on stress analysis methodology, and comparison of salt and sodium. Solar Energy 160, 368 - 379.

Rodriguez-Sanchez, M., Soria-Verdugo, A., Almendros-Ibañez, J.A., Acosta-Iborra, A., Santana, D., 2014. Thermal design guidelines of solar power towers. Applied Thermal Engineering 63, 428 - 438.